Published OnlineFirst July 8, 2014; DOI: 10.1158/0008-5472.CAN-14-0008

Cancer Research

IDH1 R132H Mutation Generates a Distinct Phospholipid Metabolite Profile in Glioma

Morteza Esmaeili[1], Bob C. Hamans[2], Anna C. Navis[3], Remco van Horssen[4,5], Tone F. Bathen[1], Ingrid S. Gribbestad[1†], William P. Leenders[3], and Arend Heerschap[1,2]

Abstract

Many patients with glioma harbor specific mutations in the isocitrate dehydrogenase gene *IDH1* that associate with a relatively better prognosis. *IDH1*-mutated tumors produce the oncometabolite 2-hydroxyglutarate. Because IDH1 also regulates several pathways leading to lipid synthesis, we hypothesized that *IDH1*-mutant tumors have an altered phospholipid metabolite profile that would impinge on tumor pathobiology. To investigate this hypothesis, we performed ^{31}P-MRS imaging in mouse xenograft models of four human gliomas, one of which harbored the *IDH1*-R132H mutation. ^{31}P-MR spectra from the *IDH1*-mutant tumor displayed a pattern distinct from that of the three *IDH1* wild-type tumors, characterized by decreased levels of phosphoethanolamine and increased levels of glycerophosphocholine. This spectral profile was confirmed by *ex vivo* analysis of tumor extracts, and it was also observed in human surgical biopsies of *IDH1*-mutated tumors by ^{31}P high-resolution magic angle spinning spectroscopy. The specificity of this profile for the *IDH1*-R132H mutation was established by *in vitro* ^{31}P-NMR of extracts of cells overexpressing IDH1 or IDH1-R132H. Overall, our results provide evidence that the *IDH1*-R132H mutation alters phospholipid metabolism in gliomas involving phosphoethanolamine and glycerophosphocholine. These new noninvasive biomarkers can assist in the identification of the mutation and in research toward novel treatments that target aberrant metabolism in *IDH1*-mutant glioma. *Cancer Res; 74(17); 1–10. ©2014 AACR.*

Introduction

Diffuse gliomas are the most common malignant brain-born tumors and are incurable with present therapeutic strategies (1). These tumors are classified by the World Health Organization (WHO) as grade 2, 3, and 4 of which grade 4 glioma (glioblastoma, GBM) is the most malignant type. The current median survival from the time of diagnosis for GBMs is only 14.6 months and for lower grades between 4 and 15 years (2, 3). This highly variable survival calls for reliable prognostic biomarkers for rational decision making in clinical management. Such biomarkers have become available with the discovery that in more than 70% of grade 2 and 3 gliomas and in secondary GBMs, one of the genes for *isocitrate dehydrogenase* (*IDH1* and *IDH2*) carry specific mutations, which are associated with prolonged overall survival (4–8). IDH1, the predominantly affected enzyme (>95%), catalyzes the conversion of isocitrate into α-ketoglutarate (α-KG) in the cytosol, using NADP as electron acceptor to generate NADPH (Fig. 1A). IDH1 can also catalyze the reductive carboxylation of α-KG to isocitrate that can be further processed to citrate and acetyl- and succinyl-CoA, important anabolic precursors for lipid synthesis (9). The mutation in *IDH1*, almost always affecting arginine R132, confers a neomorphic activity to the enzyme, which results in NADPH-dependent conversion of α-KG to 2-hydroxyglutarate (2-HG; Fig. 1A; ref. 10). The mutant enzyme lacks the capacity of reductive carboxylation (11). As 2-HG accumulates in mutated tumor cells and tissues (12–14), it has attracted attention as a potential biomarker in the diagnosis and prognosis of gliomas, in particular as the high levels of 2-HG can be detected noninvasively by ^{1}H MR spectroscopy (MRS) in humans (8, 15–19).

^{1}H MRS has been explored extensively in the diagnosis and treatment evaluation of brain tumors in humans (20, 21). MR spectra of the brain show a single spectral peak for the methyl protons of small choline compounds, which are involved in the Kennedy pathway of membrane lipid synthesis and breakdown (Fig. 1B). In brain tumors, choline metabolism is adapted to the needs of higher proliferation and to the physiologic microenvironment (such as acidic extracellular pH; refs. 22, 23), and the intensity of this peak (labeled as total choline or tCho) is often increased (24). Another prominent spectral change is a

[1]Department of Circulation and Medical Imaging, Norwegian University of Science and Technology (NTNU), Trondheim, Norway. [2]Department of Radiology, Radboud University Medical Center, Nijmegen, the Netherlands. [3]Department of Pathology, Radboud University Medical Center, Nijmegen, the Netherlands. [4]Department of Cell Biology, Radboud Institute for Molecular Life Sciences, Nijmegen, the Netherlands. [5]Department of Clinical Chemistry and Hematology, St. Elisabeth Hospital, Tilburg, the Netherlands.

Note: Supplementary data for this article are available at Cancer Research Online (http://cancerres.aacrjournals.org/).

†Deceased.

W.P. Leenders and A. Heerschap contributed equally to the article.

Corresponding Author: Morteza Esmaeili, Norwegian University of Science and Technology (NTNU), NTNU/ISB, P.O. Box 8905, 7491, Trondheim, Norway. Phone: 47-451-22-970 Fax: 47-728-28-372; E-mail: m.esmaeili@ntnu.no

doi: 10.1158/0008-5472.CAN-14-0008

Published OnlineFirst July 8, 2014; DOI: 10.1158/0008-5472.CAN-14-0008

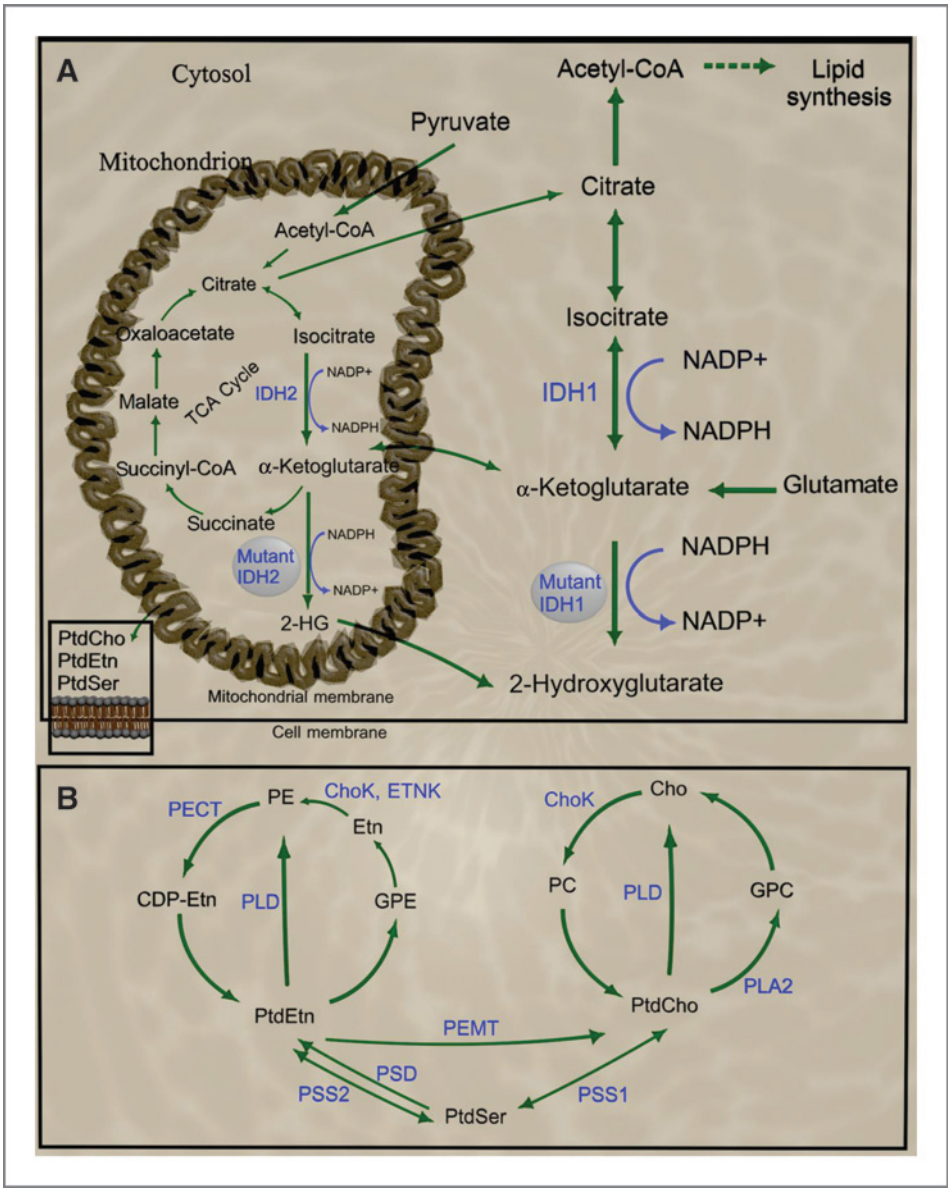

Figure 1. Schemes of metabolism involved in 2-HG biosynthesis (A), and of choline and ethanolamine phospholipid metabolism (B). Arrows, metabolic pathways. A, IDH1/2 catalyze oxidative decarboxylation of isocitrate to α-KG using $NADP^+$ as a cofactor to generate NADPH and CO_2. Mutations in these genes generate the oncometabolite 2-HG by consuming NADPH, and have an impact on intracellular signaling and epigenetics. The citrate generated via the TCA cycle contributes to the lipid synthesis. This pathway can be interrupted by mutations in *IDH1* and/or *IDH2* genes. Subsequent metabolism of citrate produces acetyl-CoA for fatty acid and/or lipid synthesis, and other intermediates such as oxaloacetate and malate in TCA cycle. B, metabolic pathways of PtdCho and PtdEtn. Acyl-CoA, acyl-coenzyme A; Etn, ethanolamine; CDP-Etn, cytidinediphosphate ethanolamine; PtdSer, phosphatidylserine; ChoK, choline kinase (EC 2.7.1.32); ETNK, ethanolamine kinase (EC 2.7.1.82); cPLA2, cytosolic phospholipase A2 (EC 3.1.1.4); PLC, phospholipase C (EC 3.1.4.3); PSD, phosphatidylserine decarboxylase (EC 4.1.1.65); PSS1, phosphatidylserine synthase I (EC Ptdss1); PSS2, phosphatidylserine synthase II (EC Ptdss2); PEMT, phosphatidylethanolamine N-methyltransferase (EC 2.7.8.29).

decrease of the peak for the methyl protons of N-acetyl aspartate (NAA), a neuronal marker compound, reflecting replacement of neurons by glial tumor cells (25). The tCho/NAA ratio is, therefore, often used as a biomarker for tumor load and malignancy in gliomas (26–28). The intensity of the tCho peak also correlates with cell density, and may be related to gliosis (29, 30).

To understand in more detail what determines the tCho peak intensity, an analysis of each contributing component is needed. This is possible with ^{1}H MRS of *ex vivo* biopsy material, which has a better spectral resolution than *in vivo* MRS and allows the separation of tCho into peaks for phosphocholine (PC), glycerophosphocholine (GPC), and free choline (24). *Ex vivo* ^{1}H MRS or high-resolution magic angle spinning (HR-MAS) spectroscopy has revealed that PC and GPC contribute importantly to the increase of tCho in brain tumors and also uncovered more subtle relationships of choline compounds with tumor features, in particular with tumor grade (31–34).

Direct *in vivo* detection of PC and GPC is possible by ^{31}P MRS, which also enables detection of phosphoethanolamine (PE) and glycerophosphoethanolamine (GPE), thereby providing a more complete picture of *in vivo* phospholipid metabolism (35). Because ^{31}P MRS is less sensitive than ^{1}H MRS and requires dedicated radiofrequency probes, it has been less used to examine phospholipid metabolites *in vivo* in brain tumors (36, 37). However, the increased access to high-field (pre-) clinical MR scanners, which improves ^{31}P MRS sensitivity and resolution, invigorates its further exploration in studies of tumor phospholipid metabolism.

As α-KG and NADPH are important components for lipogenesis (38, 39) and as the mutated IDH enzyme consumes both compounds and lacks reductive carboxylation capacity,

Published OnlineFirst July 8, 2014; DOI: 10.1158/0008-5472.CAN-14-0008

we hypothesized that phospholipid metabolism is altered in *IDH1*-mutated glioma. To test this hypothesis, we applied *in vivo* ^{31}P MR spectroscopic imaging (MRSI) to four unique and representative human glioma models growing orthotopically in mice (40), one carrying the *IDH1*-R132H mutation (41). The spectral findings were verified by ^{31}P NMR analyses of tumor tissue extracts. To examine the causal relationship of the spectral profiles to expression of the mutated enzyme, we also performed ^{31}P NMR on extracts of glioma cell lines, stably expressing wild-type or mutated *IDH1*. Finally, we tested if similar phospholipid profiles occur in human gliomas by performing ^{31}P HR-MAS MRS of biopsies of gliomas in patients with and without *IDH1* mutation.

Materials and Methods

Animals

Balb/c nu/nu mice were obtained from Janvier and housed in filter-top cages under specific pathogen-free conditions. Animals were fed a standard diet with food and water *ad libitum*. A 12-hour light, 12-hour dark day–night regimen was applied. All procedures and experiments involving animals were approved by The National Animal Research Authority, and carried out according to the European Convention for the Protection of Vertebrates used for scientific purposes.

Glioma xenografts

Glioma xenografts were injected in the brain of female Balb/c nu/nu mice (6–10 weeks of age, $n > 4$ for each individual xenograft line), as described previously (40). Two xenograft lines, labeled E468 and E473, were originally derived from human GBM biopsies, whereas E434 and E478 were established from high-grade oligodendroglioma specimens. The E478 xenograft model contains the heterozygous *IDH1*-R132H mutation (41). All xenografts grow via diffuse infiltration, whereas the E434 model additionally presents with some compact growth (40).

Development of IDH1 (-R132H)–expressing cell lines

To generate IDH1 and IDH1-R132H–expressing U251MG glioma cell lines, human IDH1 cDNA (accession number, BC093020, ImaGenes) in pBluescript plasmid was used for site-directed mutagenesis using the QuickChange Site-Directed Mutagenesis Kit (Stratagene/Agilent). Primers containing the critical IDH1-G395A mutation were 5′-CCT ATC ATC ATA GGT CAT CAT GCT TAT GGG GAT CAA TAC AGA GC-3′ (forward) and 5′-GC TCT GTA TTG ATC CCC ATA AGC ATG ATG ACC TAT GAT GAT AGG-3′ (reverse, mutated bases are underlined). After mutant strand synthesis, DNA of both wild-type and mutant IDH1 was amplified using primers 5′-GAA TTC ATG TCC AAA AAA ATC AGT GGC GG-3′ (forward) and 5′-GGA TCC TTA AAG TTT GGC CTG AGC-3′ (reverse) and cloned into the *Eco*R1 and *Bam*H1 sites of a customized pENTR/U6 vector (Invitrogen). Both pENTRY/U6 plasmids were recombined with pLenti/DEST (Invitrogen) using LR clonase-II for 6 hours at 25°C, proteinase-K treated for 10 minutes at 37°C and transformed into One Shot Stbl3 *E. coli*. Plasmids from overnight grown colony cultures were isolated using the Plasmid Midi Kit from Qiagen. To produce lentivirus, 293FT cells were transfected using Lipofectamine 2000 (Invitrogen) and the pLenti/DEST DNA was mixed with ViraPower Packaging mix (Invitrogen). After overnight incubation, medium was replaced and lentivirus-containing medium was harvested after 72 hours, filtered, and used to infect U251MG glioma cells for 6 hours with addition of polybrene (5 μg/mL). After 48 hours, medium was replaced with medium containing blasticidin (10 μg/mL; Invitrogen) and cells were kept under selection for at least 2 weeks. IDH1 expression in U251-IDH1 and U251-IDH1R132H cells was analyzed by Western blotting using a specific antibody recognizing the mutation (42).

Cells were grown in DMEM containing high glucose, supplemented with 10% FCS and penicillin/streptomycin (100 U/mL). ^{31}P MRS was performed on extracts of U251 cells (parental, *IDH*-WT and *IDH1*-R132H; $n = 5$ per cell line, $>1.5 \times 10^7$ cells per sample) as described below.

Surgical specimens of glioma patients

Surgical specimens were collected from 6 *IDH*-wild-type (*IDH*-WT) glioma patients (4 GBM, 1 anaplastic astrocytoma, and 1 diffuse astrocytoma), and from 5 *IDH1*-R132H tumors (3 GBM, 1 anaplastic astrocytoma, and 1 diffuse astrocytoma). *IDH* mutation was identified by anti-IDH1-R132H immunostaining as described previously (34). Directly after surgical excision, samples were snap frozen and stored for later analysis

In vivo ^{31}P 3D MRSI acquisition and analysis

All *in vivo* MR experiments were performed on a preclinical 7T MR system (Bruker ClinScan) operating at 121.7 MHz for ^{31}P MRS. The phosphorus spectra were acquired using a homebuilt 16-mm transmit/receive quadrature coil in combination with a solenoid ^{1}H surface coil (20 mm in diameter). The animals were subjected to MRSI when evident signs of tumor burden (especially evident weight loss, neurologic defects) were present. A control group consisting of healthy Balb/c nu/nu animals ($n = 3$) was also included. Animals were placed in prone position and anesthetized by 1.5% isoflurane (Abott) and a mixture of O_2 and N_2O inhalation. The animal's body temperature was maintained at 37.5°C applying warm air circulation and physiologic monitoring (Small Animal Instrument Inc.) to assess respiration and temperature. After obtaining a localizer image, T2-weighted multi spin-echo images in three orthogonal orientations of the brain were acquired. First- and second-order shimming was performed using FASTMAP (43). The MRSI field of view (FOV) and matrix size were then selected carefully reviewing T2-weighted images to cover hyperintense areas within the tumor tissues (Fig. 2). Three-dimensional ^{31}P MR spectroscopy was performed using a 3D MRSI pulse acquire sequence with an adiabatic BIR-4 45° excitation pulse (44), a repetition time (TR) of 1500 milliseconds, Hanning-weighted cartesian k-space sampling with 196 signal averages at the centre of k-space, 2,048 data points over a spectral width of 4,868 Hz and a total acquisition time of 2 hours. The FOV of 24 mm × 24 mm × 24 mm with an 8 × 8 × 8 data matrix and Hamming filtering resulted in a nominal voxel size of about 5 mm^3.

After the MR exams, the animals were sacrificed by cervical dislocation, the brains removed and separated in two halves,

Published OnlineFirst July 8, 2014; DOI: 10.1158/0008-5472.CAN-14-0008

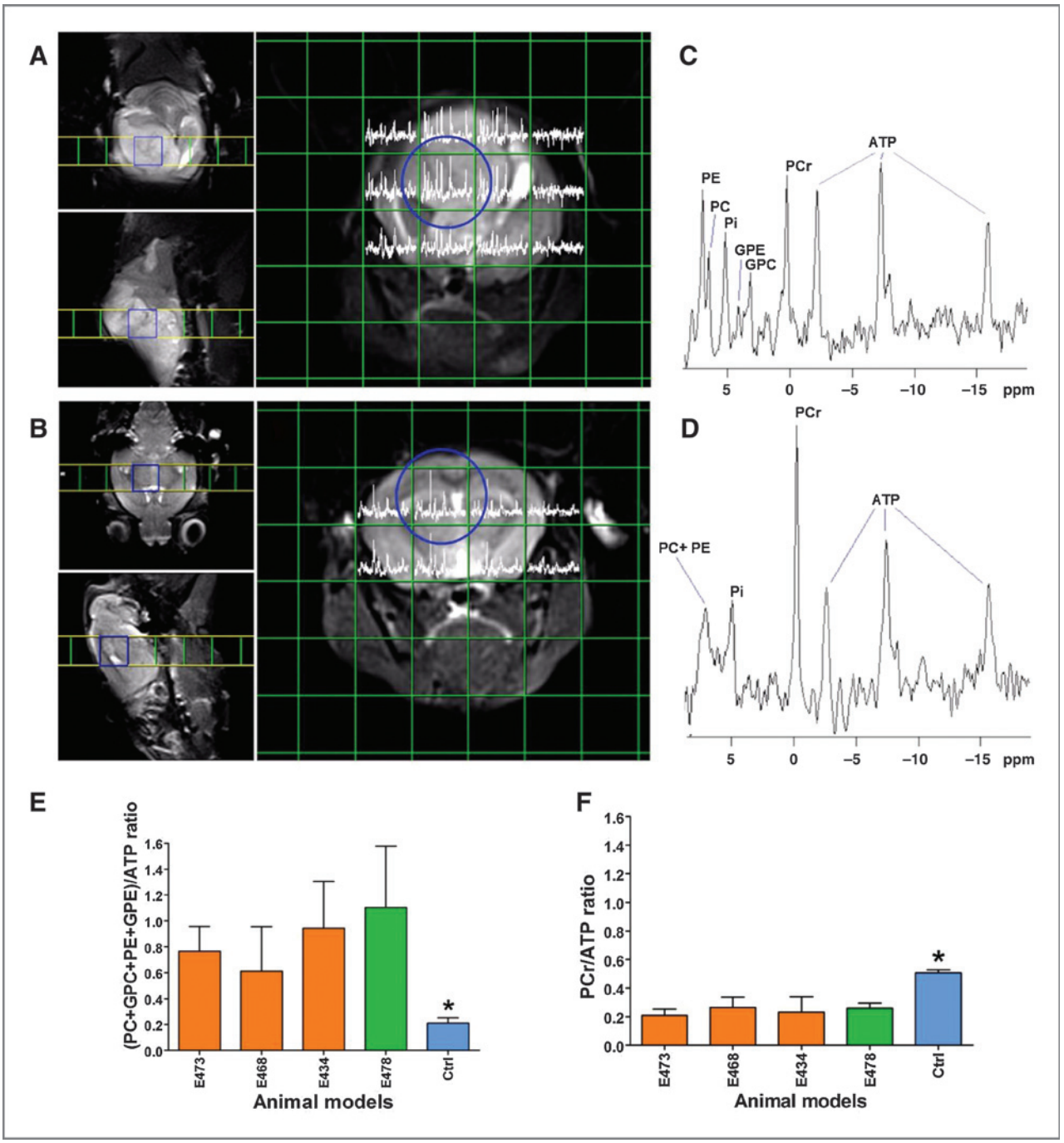

Figure 2. ^{31}P MRSI of the mouse brain with and without tumor. Orthogonal T2-weighted MR images of a mice brain with an E434 tumor (top, A) and a normal mouse brain (bottom, B) in axial, coronal, and sagital views, and corresponding ^{31}P MR spectra of 27 mm^3 nominal voxels from the 3D ^{31}P MRSI data (C and D). E and F, bar plot of the (PC + GPC + PE + GPE)/ATP (E) and PCr/ATP (F) signal ratios of tumor types growing in mouse brain ($n = 19$) and of normal mouse brain (Ctrl, $n = 3$). Chemical shift is referenced to the GPC resonance at 3.04 ppm. The assigned peaks are (from left to right); PE, phosphoethanolamine; PC, phosphocholine; Pi, inorganic phosphate; GPE, glycerophosphoethanolamine; GPC, glycerophosphocholine; PCr, phosphocreatine; ATP, adenosine tri-phosphates. *, $P < 0.05$.

which were frozen in liquid nitrogen for subsequent *in vitro* MRS analyses. Remaining brain tissue was formalin fixed and paraffin embedded for further histopathology analysis.

All *in vivo* MR spectra were analyzed using the jMRUI software (45) and signals fitted with a Lorentzian lineshape, except the J-coupled signals of ATP, which were fitted with a Gaussian shape, using the Advanced Method for Accurate, Robust and Efficient Spectral fitting method (46). Before fitting, spectral processing was performed, including manual phase correction, zero-filling (4,096 points), and line-broadening of 20 Hz.

Published OnlineFirst July 8, 2014; DOI: 10.1158/0008-5472.CAN-14-0008

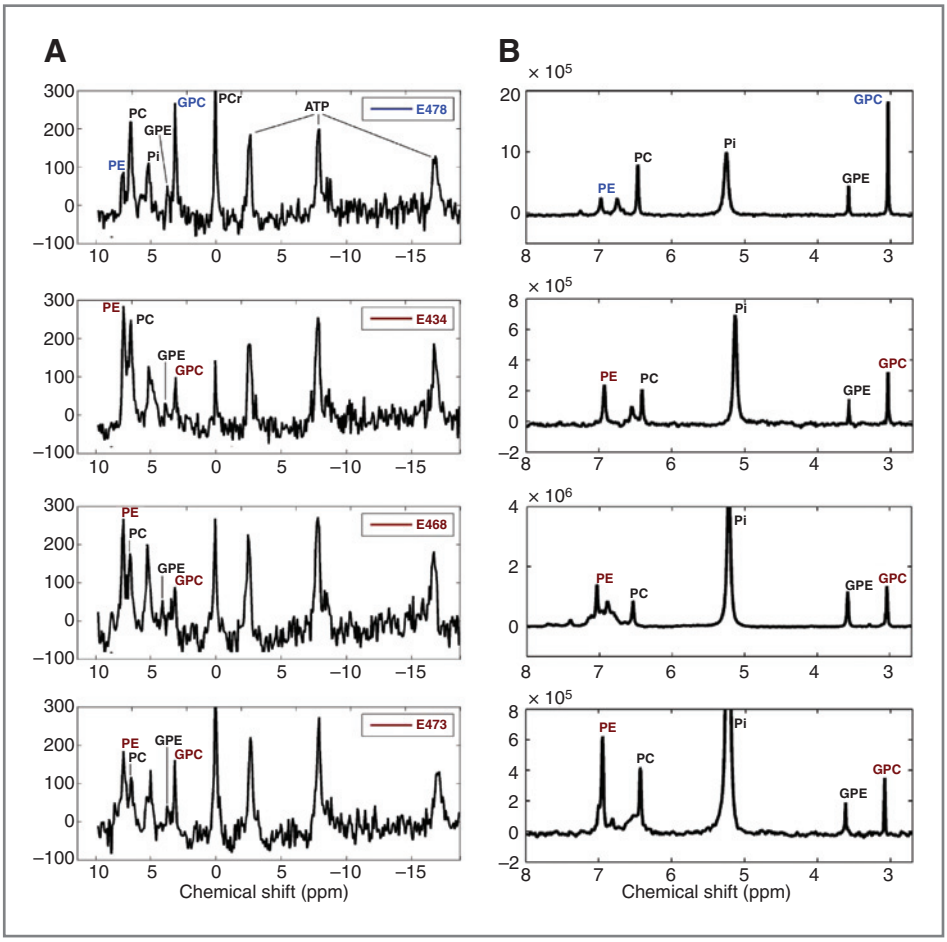

Figure 3. *IDH1*-mutated E478 xenografts show a distinct ^{31}P-spectral pattern. A, *in vivo* ^{31}P MR spectra obtained from four human glioma xenograft tumor lines growing in the mouse brain (*IDH1*-mutated xenograft E478, and *IDH1*-WT E434, E473, and E468). In the *IDH1*-mutated xenograft, GPC is highly elevated and PE decreased compared with the wild-types. B, representative *in vitro* 243.5 MHz (^{1}H-decoupled) ^{31}P MR spectra of tissue extracts of these tumors; from top to bottom the *IDH1*-mutated E478, and the *IDH1*-WT lines E434, E468, and E473. The chemical shift reference is the GPC resonance at 3.04 ppm.

Nuclear magnetic resonance acquisition and analysis of *in vitro* and *ex vivo* samples

Frozen brain tissue samples from the glioma xenografts and U251 cell pellets were extracted using perchloric acid as described in detail previously (47). The neutralized extracts were lyophilized and kept at −80°C until being dissolved in 600 μL of D_2O. After final pH adjustments with potassium hydroxide (KOH), *in vitro* ^{31}P NMR spectra of extracts were acquired using a Bruker spectrometer (Bruker Avance III 600 MHz/54 mm US-Plus) equipped with a multinuclear QCI CryoProbe (Bruker BioSpin GmbH) operating at 243.5 MHz for ^{31}P MRS. High-resolution ^{31}P NMR spectra of the water-soluble metabolites were obtained with proton decoupling during acquisition, a 30° flip angle, 8,192 free induction decays (FID), TR = 4 seconds, spectral width of 14,577 Hz into 36,864 data points in time domain.

^{31}P HR-MAS spectroscopy was carried out using a 600-MHz spectrometer (Bruker Avance III 600 MHz/54 mm US-Plus) equipped with a triple ^{1}H/^{13}C/^{31}P MAS probe (Bruker BioSpin GmbH). The frozen specimens from human brain tumors were thawed and cut on an ice-pad. Tissue samples were gently loaded into 30-μL disposable inserts filled with 3 μL ^2H_2O (Sigma-Aldrich GmbH) for the ^{2}H lock. The inserts were then placed into a 4-mm diameter ZrO_2 MAS rotor (Bruker BioSpin GmbH). The MAS rotors were spun at 5 kHz and maintained at 4°C to minimize enzymatic activities within the tissue samples.

All *in vitro* and *ex vivo* spectra were processed using the Bruker TopSpin V3.0 software (Bruker BioSpin GmbH). The accumulated FIDs were Fourier transformed after application of 3 Hz exponential line broadening. Automatic phase and linear baseline corrections were performed. The GPC peak (at 3.04 ppm) in ^{31}P MR spectra was used as references for chemical shift calibration. Following standard processing, peak areas of phosphorylated metabolites were calculated by peak fitting (PeakFit V4.12; SeaSolve Software Inc.) using a combination of Gaussian–Lorentzian lineshapes (Voigt area). Metabolite concentrations were calculated from peak areas.

Statistical analysis

The difference in the mean value of selected metabolite ratios were statistically assessed using a two-tailed unpaired Mann–Whitney test (Prism GraphPad V 4.03 Software Inc.) and the differences were considered statistically significant for P values < 0.05. All results are represented as mean ± standard deviation (SD).

Results

In vivo 3D ^{31}P MRSI of human glioma xenografts

Tumors in the brain present as hyperintense signal areas on T2-weighted MR images (compare the tumor-containing brain

Published OnlineFirst July 8, 2014; DOI: 10.1158/0008-5472.CAN-14-0008

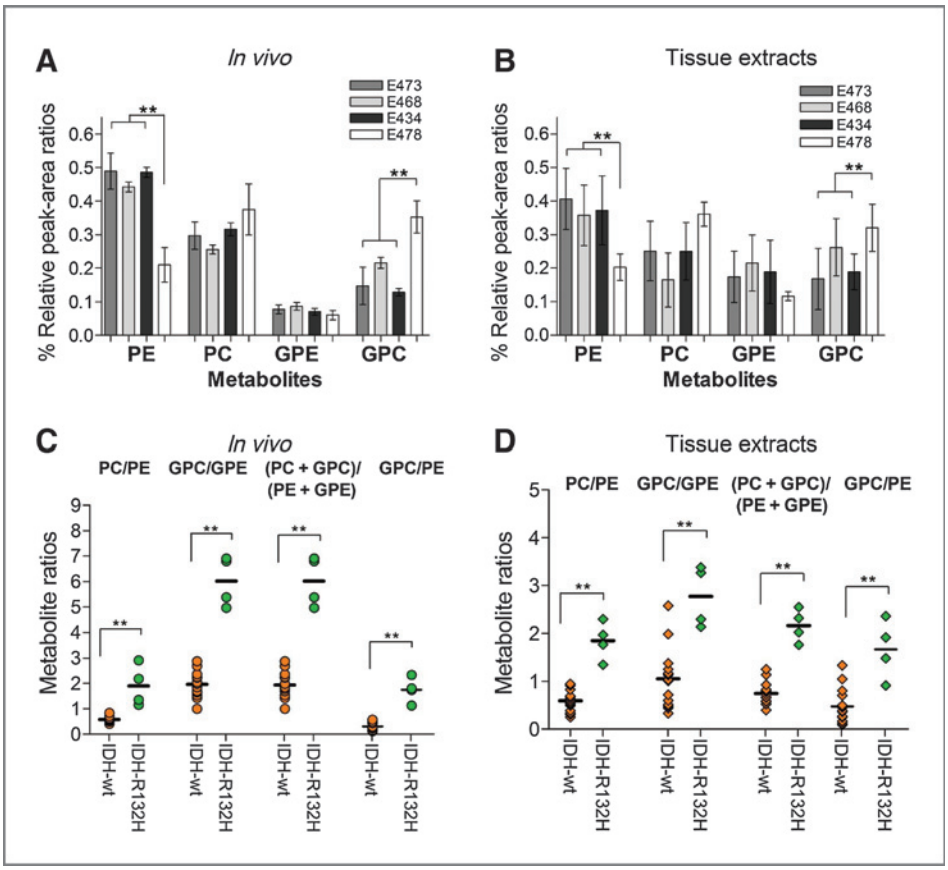

Figure 4. Relative tissue levels of MR detectable phospholipids in brain xenograft models. Metabolite signal integrals normalized to the total integral of detectable phospholipids signals in ^{31}P MR spectra obtained from (A) *in vivo* mutant glioma xenograft E478 ($n = 4$) and wt xenografts ($n = 5$ for each) and (B) from tissue extracts of xenograft tissue extracts ($n = 4$ for E478 and $n = 5$ for the other tumor lines). Values are presented as mean ± SD. Scatter plot of metabolite ratios obtained from ^{31}P spectra measured (C) from tumors in mouse brain and (D) from extracted tumor tissue. The metabolite ratios of *IDH1*-WT tumor lines; E473 + E468 + E434 (orange, $n = 15$) were compared with the *IDH1*-mutated tumor line E478 (green, $n = 4$). The *y*-axis values indicate the mean and SD; **, $P < 0.01$.

in Fig. 2A with the normal brain in Fig. 2B), and we used these images for voxel positioning. The ^{31}P MR spectra of voxels of interest selected from the 3D MRSI dataset of this brain showed resolved resonances for a number of compounds, including ATP, phosphocreatine (PCr), GPC and GPE, inorganic phosphate (Pi), PC, and PE. The ^{31}P-spectral profiles of tumor voxels in all four xenograft models differed from those obtained from voxels in comparable brain areas in non–tumor-bearing animals (compare Fig. 2C with 2D). The relative phosphor signal integrals of choline and ethanolamine compounds were increased, as represented by a significantly higher (PC + GPC + PE + GPE)/ATP ratio for all tumor types ($P < 0.05$; Fig. 2E). This total relative phospholipid content was not different among the tumor models. In addition, a significantly decreased PCr/ATP signal ratio was observed in tumor tissues compared with the healthy mouse brain tissues ($P < 0.05$; Fig. 2F).

Among the four human glioma lines, the E478 tumor exhibited a deviating spectral profile in the 2 to 8 ppm range (Fig. 3A and B). For a quantitative assessment, we first determined for each metabolite resonance its integral normalized to the sum of those of all phospholipid metabolite resonances (see Fig. 4A and B). This revealed a significant decrease of the PE resonance of the *IDH1*-mutant E478 xenograft compared with those of the *IDH1*-WT xenografts ($P = 0.003$). A significant increase was observed for the GPC resonance of E478 compared with *IDH1*-WT tumors ($P = 0.003$). Furthermore, the PC peak of E478 showed a trend for an increase compared with the PC of the other tumors ($P = 0.08$). The GPE resonance did not differ between the tumors. In concordance with the *in vivo* results, we observed very similar differences between ^{31}P NMR spectra of tumor extracts from *IDH1*-mutant and wild-type xenografts (Fig. 3B). Again, PE was reduced and GPC increased in E478 extracts compared with those of the other models ($P = 0.004$ and 0.01 respectively; Fig. 4B)

These findings suggest that sensitive biomarkers associated with the presence of *IDH1* mutations would be represented by the peak ratios PC/PE, GPC/GPE, GPC/PE, and (PC + GPC)/(PE + GPE). A quantitative assessment of mean *in vivo* metabolite ratios obtained from all xenograft models showed that these ratios in the E478 xenograft were more than 2-fold higher than those of the other xenografts ($P < 0.01$ for all ratios; Fig. 4C). Similar findings were observed for these ratios obtained from spectra of tumor tissue extracts (Fig. 4D).

Phospholipid metabolite ratios involving PE and GPC are similarly altered in cell lines and human glioma with an *IDH1* mutation

To investigate how specific the phospholipid metabolite changes are for the *IDH1* mutation, we measured *in vitro* ^{31}P NMR spectra of extracts of a set of U251-MG cell lines overexpressing either wild-type or mutant *IDH1* (see Fig. 5A–C). The *IDH1*-R132H–expressing U251-MG cells showed

Published OnlineFirst July 8, 2014; DOI: 10.1158/0008-5472.CAN-14-0008

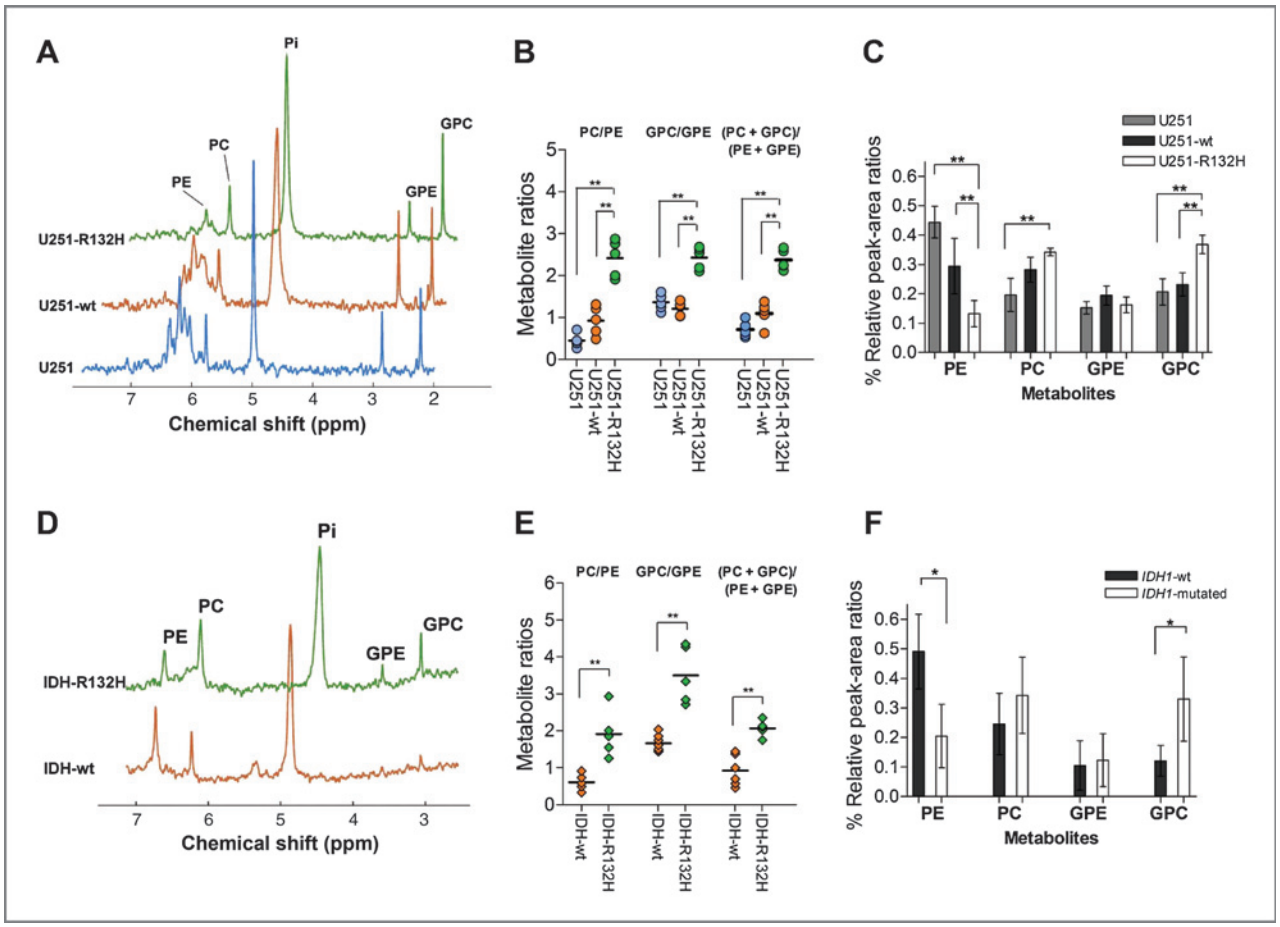

Figure 5. ^{31}P NMR spectra of U251MG cell extracts and ^{31}P HR-MAS MR spectra of surgical biopsies from patients with glioma. A, representative ^{31}P NMR spectra of cell extracts show similar ^{31}P-spectral features as observed for the *in vivo* growing brain xenografts. Relatively decreased PE and increased GPC resonances identify the mutant cell line (U251-R132H) from wild-type cell lines (U251-WT) and U251MG control cells (U251). The green and orange colored spectra are shifted to the right for a better visualization. B, the PC/PE, GPC/GPE, and (PC + GPC)/(PE + GPE) ratios are significantly increased in the U251-R132H cell line compared with the U251-WT and U251 cells. C, phospholipid levels measured from ^{31}P MR spectra of U251 cell extracts. D, representative ^{31}P HR-MAS MR spectra of glioma patient biopsies. E, the levels of PC/PE, GPC/GPE, (PC + GPC)/(PE + GPE) ratios in *IDH1*-R132H glioma patients are consistent with preclinical results. F, phospholipid metabolite levels measured in glioma patient tissues samples. The *y*-axis values indicate the mean and SD; *, $P < 0.05$; **, $P < 0.01$.

significantly higher PC/PE and GPC/GPE levels than U251-IDHwt ($P < 0.001$) and U251-MG control cell lines ($P < 0.01$ for both ratios; Fig. 5B). The U251-R132H also showed a significantly higher (PC + GPC)/(PE + GPE) ratio ($P < 0.01$; Fig. 5B).

Finally, we investigated if these *IDH*-mutant specific spectral findings could be validated in human gliomas. For this purpose, we obtained ^{31}P HR-MAS spectra of human glioma specimens. Again, ^{31}P spectral profiles in *IDH1*-mutant gliomas (Fig. 5D–F) were obtained that were characterized by significant elevations in PC/PE, GPC/GPE, and (PC + GPC)/(PE + GPE) ratios ($P < 0.01$ for all ratios) as compared with *IDH1*-WT glioma specimens (Fig. 5E).

Discussion

In this study, we tested the hypothesis that *IDH1* mutations affect the phospholipid metabolite profile of tumors by using *IDH1*-R132H E478 xenografts (41). Our major finding is that gliomas with an *IDH1* mutation indeed have a phospholipid profile, which differs from that in gliomas with wild-type *IDH1*. This is reflected most clearly in relatively higher GPC and lower PE tissue levels, resulting in more than two-fold higher PC/PE, GPC/GPE, and GPC/PE ratios for the *IDH1* mutants. ^{31}P nuclear magnetic resonance (NMR) of tumor tissue extracts obtained from the same animals confirmed the *in vivo* findings. Moreover, ^{31}P NMR of extracts of U251 cells, stably expressing recombinant *IDH1*-R132H also yielded increased PC/PE and GPC/GPE ratios compared with *IDH*-WT cells, proving that these changes are related to the *IDH1* mutation. Finally, ^{31}P HR-MAS of surgical biopsies of human brain tumors identified similar *IDH* mutation–specific phospholipid metabolite patterns.

An increased GPC level has been detected by mass spectrometry in oligodendroglioma cells expressing the *IDH1* mutation as compared with wild-type cells (14), and a positive correlation of GPC with 2HG was found by HR-MAS of *ex vivo*

Published OnlineFirst July 8, 2014; DOI: 10.1158/0008-5472.CAN-14-0008

biopsies of low-grade tumors with the mutation (18). Elevated GPC has been associated with grade 2 and 3 gliomas (32–34). Because the majority of these have the *IDH1* mutation and elevated GPC is associated with 2-HG (18), this suggests that GPC levels have a causal relationship with the mutation, which is in agreement with our findings. There is much less known for PE. Its resonances in ^{1}H MR spectra are not well resolved. Data from ^{31}P HR-MAS studies of biopsies indicate that PE is decreased in low-grade gliomas (34, 48), but the only report describing PE in relation to the *IDH1* mutation indicates a positive correlation with 2-HG, as detected by ^{1}H HR-MAS (18). As ^{31}P NMR of the GBM cell line GS-2 also showed low PE to PC and high GPC to GPE ratios (49), it would be of interest to investigate whether this line also carries the *IDH* mutation.

For all tumors in the mouse brain, we detected a decreased PCr/ATP ratio, which is in line with findings in ^{31}P MRS of human tumors and indicates an altered energy metabolism (37, 50).

IDH1 mutations are confined to low-grade and secondary high-grade glioma GBM (4, 5) and confer a relatively good prognosis to patients suffering from these tumors (6, 7, 51). Despite their frequent occurrence, glioma xenografts carrying these mutations are very scarce (41, 52, 53), and *in vitro* propagation of *IDH1*-mutated glioma cell lines is challenging (54). Interestingly, and in line with clinical observations, E478 xenografts present with lower proliferation rates than *IDH*wt counterparts, as established via the Ki67 index, and mice carrying these xenografts have a longer survival time than mice carrying *IDH*wt xenografts (see Supplementary Materials). A correlation between longer survival, lower Ki67, and lower PC/GPC ratio has also been observed in human patients with glioma (32, 34).

^{31}P MRSI of brain tumors and imaging biomarkers for *IDH1* mutation

In this study, we demonstrate that ^{31}P MR spectra of the mouse brain can be obtained with a good signal-to-noise ratio (SNR) by 3D MRSI on a 7T magnet with a dedicated ^{31}P coil. Moreover, at this field strength, resolved signals for individual choline- and ethanolamine-containing metabolites can be detected. This is also possible for human brain at clinical field strengths (1.5–3T) using ^{1}H decoupling (35, 37) and ^{1}H-^{31}P polarization transfer to enhance sensitivity (55, 56). Thus, it is worthwhile to investigate if ratios of PE and GPC signals can be used as biomarkers to assist in the noninvasive metabolic characterization of *IDH* mutations in patients with glioma brain tumors. This may be used in the assessment of the effect of inhibitors of the mutated IDH enzyme (57).

It is known that human glioma cells with an *IDH1* mutation accumulate 2-HG (12–14). We confirmed the presence of 2-HG in our E478 model and in IDH-R132H–overexpressing U251 cells, by both LC/MS (41) and 1D and TOCSY ^{1}H MRS (see Supplementary Materials). This accumulation enables the detection of 2-HG by ^{1}H MRSI, by which patients with this mutation can be identified (15, 17). However, spectral overlap hampers discrimination of 2-HG signals from those of glutamine, glutamate, and gamma-amino butyric acid, even with peak fitting using prior knowledge and optimal echo times. This may be overcome by spectral editing or 2D ^{1}H MRS, but at the expense of increased complexity and longer scan times or low SNR (17). Moreover, in clinical practice, all these methods to detect 2-HG may fail due to suboptimal field homogeneity. As the resolved detection of ^{31}P signals is less prone to field inhomogeneities, the distinct phospholipid metabolite profiles in *IDH1*-mutated gliomas may have a role in the identification of this mutation.

Biologic meaning of the change in phospholipid levels in *IDH1*-mutated glioma

Many enzymes that are involved in lipid biosynthesis depend on appropriate levels of cytosolic NADPH and acetyl-CoA. The activity of IDH1 is an important source for cytosolic NADPH in the brain (ref. 51; see also Fig. 1A) and only for this reason, mutations in this enzyme are expected to affect lipid synthesis. This impact will be augmented by the fact that IDH1 is also involved in the reductive carboxylation of α-KG to isocitrate, especially under hypoxic conditions, isocitrate being the building block for lipids via generation of acetyl- and succinyl-CoA. In mutated *IDH1*, this activity is lost (11). Evidently, according to this model, *IDH1*-mutated tumor cells are subject to high metabolic stress, and cells need to adapt to this stress to facilitate survival and tumor progression (58). In a previous report we described that E478 xenografts, despite the *IDH1* mutation, do not have significantly decreased α-KG levels and present with densely packed mitochondria. On the basis of these findings, we postulated that *IDH1*-mutated tumor cells rescue the IDH1 defect by upregulating mitochondrial biosynthesis and concomitantly IDH2 activity, followed by transport of mitochondrial α-KG and NADPH to the cytosol (41). To accommodate mitochondrial biosynthesis, membrane synthesis is required. The altered steady-state levels of some phospholipid metabolites in *IDH1*-mutated gliomas may be related to rapid incorporation of precursors in phosphatidylcholine (PtdCho) and phosphatidylethanolamine (PtdEtn), the most abundant membrane compounds (59). An interesting question that directly follows, is whether energy production in *IDH1*-mutated gliomas is balanced more toward oxidative phosphorylation than to aerobic glycolysis (the Warburg phenomenon; ref. 60). Such considerations may eventually lead to therapeutic handles.

In conclusion, we provide evidence that *IDH1* mutations result in distinct alterations in lipid metabolism that can be detected noninvasively by ^{31}P MRSI. These may serve as a complementary biomarker to characterize the metabolic status of *IDH1*-mutated gliomas during evaluation of anticancer targeted therapies and in tumor diagnosis. Increased availability to higher field strength MR systems (3 and 7 T) and dedicated ^{31}P coils hold promise for clinical translation of the ^{31}P MRSI method. Further research is needed to fully elucidate the roles of PE and GPC, such as their involvement in mitochondrial membrane synthesis.

Disclosure of Potential Conflicts of Interest

No potential conflicts of interest were disclosed.

Authors' Contributions

Conception and design: M. Esmaeili, W.P. Leenders, A. Heerschap
Development of methodology: M. Esmaeili, W.P. Leenders, A. Heerschap

Acquisition of data (provided animals, acquired and managed patients, provided facilities, etc.): M. Esmaeili, B.C. Hamans, A.C. Navis, R. van Horssen
Analysis and interpretation of data (e.g., statistical analysis, biostatistics, computational analysis): M. Esmaeili, B.C. Hamans, A.C. Navis, T.F. Bathen, W.P. Leenders, A. Heerschap
Writing, review, and/or revision of the manuscript: M. Esmaeili, B.C. Hamans, A.C. Navis, T.F. Bathen, I.S. Gribbestad, W.P. Leenders, A. Heerschap
Administrative, technical, or material support (i.e., reporting or organizing data, constructing databases): M. Esmaeili, I.S. Gribbestad, A. Heerschap
Study supervision: M. Esmaeili, T.F. Bathen, I.S. Gribbestad, W.P. Leenders, A. Heerschap

Acknowledgments

The authors thank A. Veltien and J. van der Laak for technical assistance with MR measurements and KS400 software, respectively, and Marieke Willemse for generating the U251-cell lines. The authors also thank Jeroen Mooren and Bianca Lemmers van de Weem for their assistance during the animal experiments.

Grant Support

This research was also supported by NWO investment grants 91106021 and BIG (VISTA).

The costs of publication of this article were defrayed in part by the payment of page charges. This article must therefore be hereby marked *advertisement* in accordance with 18 U.S.C. Section 1734 solely to indicate this fact.

Received January 6, 2014; revised April 28, 2014; accepted May 26, 2014; published OnlineFirst July 8, 2014.

References

1. Clarke J, Butowski N, Chang S. Recent advances in therapy for glioblastoma. Arch Neurol 2010;67:279–83.
2. Louis DN, Ohgaki H, Wiestler OD, Cavenee WK, Burger PC, Jouvet A, et al. The 2007 WHO classification of tumours of the central nervous system. Acta Neuropathol 2007;114:97–109.
3. Stupp R, Hegi ME, Gilbert MR, Chakravarti A. Chemoradiotherapy in malignant glioma: standard of care and future directions. J Clin Oncol 2007;25:4127–36.
4. Parsons DW, Jones S, Zhang X, Lin JC, Leary RJ, Angenendt P, et al. An integrated genomic analysis of human glioblastoma multiforme. Science 2008;321:1807–12.
5. Yan H, Parsons DW, Jin G, McLendon R, Rasheed BA, Yuan W, et al. IDH1 and IDH2 mutations in gliomas. N Engl J Med 2009;360:765–73.
6. Hartmann C, Meyer J, Balss J, Capper D, Mueller W, Christians A, et al. Type and frequency of IDH1 and IDH2 mutations are related to astrocytic and oligodendroglial differentiation and age: a study of 1,010 diffuse gliomas. Acta Neuropathol 2009;118:469–74.
7. Houillier C, Wang X, Kaloshi G, Mokhtari K, Guillevin R, Laffaire J, et al. IDH1 or IDH2 mutations predict longer survival and response to temozolomide in low-grade gliomas. Neurology 2010;75:1560–6.
8. Metellus P, Coulibaly B, Colin C, de Paula AM, Vasiljevic A, Taieb D, et al. Absence of IDH mutation identifies a novel radiologic and molecular subtype of WHO grade II gliomas with dismal prognosis. Acta Neuropathol 2010;120:719–29.
9. Metallo CM, Gameiro PA, Bell EL, Mattaini KR, Yang J, Hiller K, et al. Reductive glutamine metabolism by IDH1 mediates lipogenesis under hypoxia. Nature 2012;481:380–4.
10. Dang L, White DW, Gross S, Bennett BD, Bittinger MA, Driggers EM, et al. Cancer-associated IDH1 mutations produce 2-hydroxyglutarate. Nature 2009;462:739–44.
11. Leonardi R, Subramanian C, Jackowski S, Rock CO. Cancer-associated isocitrate dehydrogenase mutations inactivate NADPH-dependent reductive carboxylation. J Biol Chem 2012;287:14615–20.
12. Dang L, Jin S, Su SM. IDH mutations in glioma and acute myeloid leukemia. Trends Mol Med 2010;16:387–97.
13. Yen KE, Bittinger MA, Su SM, Fantin VR. Cancer-associated IDH mutations: biomarker and therapeutic opportunities. Oncogene 2010;29:6409–17.
14. Reitman ZJ, Jin G, Karoly ED, Spasojevic I, Yang J, Kinzler KW, et al. Profiling the effects of isocitrate dehydrogenase 1 and 2 mutations on the cellular metabolome. Proc Natl Acad Sci U S A 2011;108:3270–5.
15. Choi C, Ganji SK, DeBerardinis RJ, Hatanpaa KJ, Rakheja D, Kovacs Z, et al. 2-hydroxyglutarate detection by magnetic resonance spectroscopy in IDH-mutated patients with gliomas. Nat Med 2012;18:624–9.
16. Pope WB, Prins RM, Albert Thomas M, Nagarajan R, Yen KE, Bittinger MA, et al. Non-invasive detection of 2-hydroxyglutarate and other metabolites in IDH1 mutant glioma patients using magnetic resonance spectroscopy. J Neurooncol 2012;107:197–205.
17. Andronesi OC, Kim GS, Gerstner E, Batchelor T, Tzika AA, Fantin VR, et al. Detection of 2-hydroxyglutarate in IDH-mutated glioma patients by *in vivo* spectral-editing and 2D correlation magnetic resonance spectroscopy. Sci Transl Med 2012;4:116ra4.
18. Elkhaled A, Jalbert LE, Phillips JJ, Yoshihara HA, Parvataneni R, Srinivasan R, et al. Magnetic resonance of 2-hydroxyglutarate in IDH1-mutated low-grade gliomas. Sci Transl Med 2012;4:116ra5.
19. Esmaeili M, Vettukattil R, Bathen TF. 2-hydroxyglutarate as a magnetic resonance biomarker for glioma subtyping. Transl Oncol 2013;6:92–8.
20. Gillies RJ, Morse DL. *In vivo* magnetic resonance spectroscopy in cancer. Annu Rev Biomed Eng 2005;7:287–326.
21. Nelson SJ. Assessment of therapeutic response and treatment planning for brain tumors using metabolic and physiological MRI. NMR Biomed 2011;24:734–49.
22. Aboagye EO, Bhujwalla ZM. Malignant transformation alters membrane choline phospholipid metabolism of human mammary epithelial cells. Cancer Res 1999;59:80–4.
23. Gillies RJ, Raghunand N, Karczmar GS, Bhujwalla ZM. MRI of the tumor microenvironment. J Magn Reson Imaging 2002;16:430–50.
24. Glunde K, Bhujwalla ZM, Ronen SM. Choline metabolism in malignant transformation. Nat Rev Cancer 2011;11:835–48.
25. Bruhn H, Frahm J, Gyngell ML, Merboldt KD, Hanicke W, Sauter R, et al. Noninvasive differentiation of tumors with use of localized H-1 MR spectroscopy *in vivo*: initial experience in patients with cerebral tumors. Radiology 1989;172:541–8.
26. Herminghaus S, Pilatus U, Moller-Hartmann W, Raab P, Lanfermann H, Schlote W, et al. Increased choline levels coincide with enhanced proliferative activity of human neuroepithelial brain tumors. NMR Biomed 2002;15:385–92.
27. Stadlbauer A, Gruber S, Nimsky C, Fahlbusch R, Hammen T, Buslei R, et al. Preoperative grading of gliomas by using metabolite quantification with high-spatial-resolution proton MR spectroscopic imaging. Radiology 2006;238:958–69.
28. Saraswathy S, Crawford FW, Lamborn KR, Pirzkall A, Chang S, Cha S, et al. Evaluation of MR markers that predict survival in patients with newly diagnosed GBM prior to adjuvant therapy. J Neurooncol 2009;91:69–81.
29. Gupta RK, Cloughesy TF, Sinha U, Garakian J, Lazareff J, Rubino G, et al. Relationships between choline magnetic resonance spectroscopy, apparent diffusion coefficient and quantitative histopathology in human glioma. J Neurooncol 2000;50:215–26.
30. Srinivasan R, Phillips JJ, Vandenberg SR, Polley MY, Bourne G, Au A, et al. *Ex vivo* MR spectroscopic measure differentiates tumor from treatment effects in GBM. Neuro Oncol 2010;12:1152–61.
31. Sabatier J, Gilard V, Malet-Martino M, Ranjeva JP, Terral C, Breil S, et al. Characterization of choline compounds with *in vitro* 1H magnetic resonance spectroscopy for the discrimination of primary brain tumors. Invest Radiol 1999;34:230–5.
32. Righi V, Roda JM, Paz J, Mucci A, Tugnoli V, Rodriguez-Tarduchy G, et al. 1H HR-MAS and genomic analysis of human tumor biopsies discriminate between high and low grade astrocytomas. NMR Biomed 2009;22:629–37.
33. McKnight TR, Smith KJ, Chu PW, Chiu KS, Cloyd CP, Chang SM, et al. Choline metabolism, proliferation, and angiogenesis in

Published OnlineFirst July 8, 2014; DOI: 10.1158/0008-5472.CAN-14-0008

nonenhancing grades 2 and 3 astrocytoma. J Magn Reson Imaging 2011;33:808–16.
34. Vettukattil R, Gulati M, Sjobakk TE, Jakola AS, Kvernmo NA, Torp SH, et al. Differentiating diffuse World Health Organization Grade II and IV astrocytomas with *ex vivo* magnetic resonance spectroscopy. Neurosurgery 2013;72:186–95.
35. Luyten PR, Bruntink G, Sloff FM, Vermeulen JW, van der Heijden JI, den Hollander JA, et al. Broadband proton decoupling in human 31P NMR spectroscopy. NMR Biomed 1989;1:177–83.
36. Albers MJ, Krieger MD, Gonzalez-Gomez I, Gilles FH, McComb JG, Nelson MD Jr, et al. Proton-decoupled 31P MRS in untreated pediatric brain tumors. Magn Reson Med 2005;53:22–9.
37. Hattingen E, Bahr O, Rieger J, Blasel S, Steinbach J, Pilatus U. Phospholipid metabolites in recurrent glioblastoma: *in vivo* markers detect different tumor phenotypes before and under antiangiogenic therapy. PLoS ONE 2013;8:e56439.
38. Shechter I, Dai P, Huo L, Guan G. IDH1 gene transcription is sterol regulated and activated by SREBP-1a and SREBP-2 in human hepatoma HepG2 cells: evidence that IDH1 may regulate lipogenesis in hepatic cells. J Lipid Res 2003;44:2169–80.
39. Yang H, Ye D, Guan KL, Xiong Y. IDH1 and IDH2 mutations in tumorigenesis: mechanistic insights and clinical perspectives. Clin Cancer Res 2012;18:5562–71.
40. Claes A, Schuuring J, Boots-Sprenger S, Hendriks-Cornelissen S, Dekkers M, van der Kogel AJ, et al. Phenotypic and genotypic characterization of orthotopic human glioma models and its relevance for the study of anti-glioma therapy. Brain Pathol 2008;18:423–33.
41. Navis AC, Niclou SP, Fack F, Stieber D, Lith Sv, Verrijp K, et al. Increased mitochondrial activity in a novel IDH1-R132H mutant human oligodendroglioma xenograft model: *in situ* detection of 2-HG and α-KG. Acta Neuropathol Commun 2013;1:18.
42. Capper D, Zentgraf H, Balss J, Hartmann C, von Deimling A. Monoclonal antibody specific for IDH1 R132H mutation. Acta Neuropathol 2009;118:599–601.
43. Gruetter R. Automatic, localized *in vivo* adjustment of all first- and second-order shim coils. Magn Reson Med 1993;29:804–11.
44. Staewen RS, Johnson AJ, Ross BD, Parrish T, Merkle H, Garwood M. 3-D FLASH imaging using a single surface coil and a new adiabatic pulse, BIR-4. Invest Radiol 1990;25:559–67.
45. Naressi A, Couturier C, Devos JM, Janssen M, Mangeat C, de Beer R, et al. Java-based graphical user interface for the MRUI quantitation package. MAGMA 2001;12:141–52.
46. Vanhamme L, van den Boogaart A, Van Huffel S. Improved method for accurate and efficient quantification of MRS data with use of prior knowledge. J Magn Reson 1997;129:35–43.
47. Gribbestad IS, Petersen SB, Fjosne HE, Kvinnsland S, Krane J. 1H NMR spectroscopic characterization of perchloric acid extracts from breast carcinomas and non-involved breast tissue. NMR Biomed 1994;7:181–94.
48. Esteve V, Celda B, Martinez-Bisbal MC. Use of 1H and 31P HRMAS to evaluate the relationship between quantitative alterations in metabolite concentrations and tissue features in human brain tumour biopsies. Anal Bioanal Chem 2012;403:2611–25.
49. Ward CS, Venkatesh HS, Chaumeil MM, Brandes AH, Vancriekinge M, Dafni H, et al. Noninvasive detection of target modulation following phosphatidylinositol 3-kinase inhibition using hyperpolarized 13C magnetic resonance spectroscopy. Cancer Res 2010;70:1296–305.
50. Hubesch B, Sappey-Marinier D, Roth K, Meyerhoff DJ, Matson GB, Weiner MW. P-31 MR spectroscopy of normal human brain and brain tumors. Radiology 1990;174:401–9.
51. Bleeker FE, Atai NA, Lamba S, Jonker A, Rijkeboer D, Bosch KS, et al. The prognostic IDH1(R132) mutation is associated with reduced NADP+-dependent IDH activity in glioblastoma. Acta Neuropathol 2010;119:487–94.
52. Luchman HA, Stechishin OD, Dang NH, Blough MD, Chesnelong C, Kelly JJ, et al. An *in vivo* patient-derived model of endogenous IDH1-mutant glioma. Neuro Oncol 2012;14:184–91.
53. Klink B, Miletic H, Stieber D, Huszthy PC, Valenzuela JA, Balss J, et al. A novel, diffusely infiltrative xenograft model of human anaplastic oligodendroglioma with mutations in FUBP1, CIC, and IDH1. PLoS ONE 2013;8:e59773.
54. Piaskowski S, Bienkowski M, Stoczynska-Fidelus E, Stawski R, Sieruta M, Szybka M, et al. Glioma cells showing IDH1 mutation cannot be propagated in standard cell culture conditions. Br J Cancer 2011;104:968–70.
55. Klomp DW, Wijnen JP, Scheenen TW, Heerschap A. Efficient 1H to 31P polarization transfer on a clinical 3T MR system. Magn Reson Med 2008;60:1298–305.
56. Wijnen JP, Scheenen TW, Klomp DW, Heerschap A. 31P magnetic resonance spectroscopic imaging with polarisation transfer of phosphomono- and diesters at 3 T in the human brain: relation with age and spatial differences. NMR Biomed 2010;23:968–76.
57. Rohle D, Popovici-Muller J, Palaskas N, Turcan S, Grommes C, Campos C, et al. An inhibitor of mutant IDH1 delays growth and promotes differentiation of glioma cells. Science 2013;340:626–30.
58. van Lith SA, Navis AC, Verrijp K, Niclou SP, Bjerkvig R, Wesseling P, et al. Glutamate as chemotactic fuel for diffuse glioma cells; are they glutamate suckers? Biochim Biophys Acta 2014;1846:66–74.
59. Farber SA, Slack BE, Blusztajn JK. Acceleration of phosphatidylcholine synthesis and breakdown by inhibitors of mitochondrial function in neuronal cells: a model of the membrane defect of Alzheimer's disease. FASEB J 2000;14:2198–206.
60. Warburg O. On the origin of cancer cells. Science 1956;123:309–14.

Cancer Research
The Journal of Cancer Research (1916–1930) | The American Journal of Cancer (1931–1940)

AACR American Association for Cancer Research

IDH1 R132H Mutation Generates a Distinct Phospholipid Metabolite Profile in Glioma

Morteza Esmaeili, Bob C. Hamans, Anna C. Navis, et al.

Cancer Res Published OnlineFirst July 8, 2014.